AMERICAN SOCIETY FOR MICROBIOLOGY | Antimicrobial Agents and Chemotherapy®

MECHANISMS OF RESISTANCE

Structural Basis of Reduced Susceptibility to Ceftazidime-Avibactam and Cefiderocol in *Enterobacter cloacae* Due to AmpC R2 Loop Deletion

Akito Kawai,[a] Christi L. McElheny,[b] Alina Iovleva,[b] Ellen G. Kline,[b] Nicolas Sluis-Cremer,[b,c] Ryan K. Shields,[b,c] Yohei Doi[a,b,c,d]

[a]Department of Microbiology, Fujita Health University School of Medicine, Toyoake, Aichi, Japan
[b]Division of Infectious Diseases, University of Pittsburgh School of Medicine, Pittsburgh, Pennsylvania, USA
[c]Center for Innovative Antimicrobial Therapy, University of Pittsburgh School of Medicine, Pittsburgh, Pennsylvania, USA
[d]Department of Infectious Diseases, Fujita Health University School of Medicine, Toyoake, Aichi, Japan

ABSTRACT Ceftazidime-avibactam and cefiderocol are two of the latest generation β-lactam agents that possess expanded activity against highly drug-resistant bacteria, including carbapenem-resistant *Enterobacterales*. Here, we show that structural changes in AmpC β-lactamases can confer reduced susceptibility to both agents. A multidrug-resistant *Enterobacter cloacae* clinical strain (Ent385) was found to be resistant to ceftazidime-avibactam and cefiderocol without prior exposure to either agent. The AmpC β-lactamase of Ent385 ($AmpC^{Ent385}$) contained an alanine-proline deletion at positions 294 and 295 (A294_P295del) in the R2 loop. $AmpC^{Ent385}$ conferred reduced susceptibility to ceftazidime-avibactam and cefiderocol when cloned into *Escherichia coli* TOP10. Purified $AmpC^{Ent385}$ showed increased hydrolysis of ceftazidime and cefiderocol compared to $AmpC^{Ent385Rev}$, in which the deletion was reverted. Comparisons of crystal structures of $AmpC^{Ent385}$ and $AmpC^{P99}$, the canonical AmpC of *E. cloacae* complex, revealed that the two-residue deletion in $AmpC^{Ent385}$ induced drastic structural changes of the H-9 and H-10 helices and the R2 loop, which accounted for the increased hydrolysis of ceftazidime and cefiderocol. The potential for a single mutation in *ampC* to confer reduced susceptibility to both ceftazidime-avibactam and cefiderocol requires close monitoring.

KEYWORDS ceftazidime, avibactam, cefiderocol, beta-lactamase

Antimicrobial resistance in Gram-negative bacteria represents one of the top public health priorities that is expected to worsen further in the absence of interventions to mitigate it. Carbapenem resistance in *Enterobacter* spp. is increasingly recognized as a clinical challenge against which few existing agents remain active. Resistance is typically due to a combination of mechanisms—derepressed production of the intrinsic AmpC β-lactamase, reduced outer membrane permeability, and augmented efflux—with or without the production of carbapenemase (1). The recent introduction of novel β-lactamase inhibitors, in particular avibactam, has significantly improved treatment of infections caused by carbapenem-resistant *Enterobacterales*, including *Enterobacter* spp. (2). Avibactam is a potent diazabicyclooctane inhibitor of class A and class C β-lactamases (Fig. 1a), the latter representing the AmpC group of enzymes. Resistance to ceftazidime-avibactam has emerged in about 10% of patients treated with this agent for infections caused by *Klebsiella pneumoniae* carbapenemase (KPC)-producing *K. pneumoniae*; this resistance is in many cases due to amino acid substitutions in the omega loop of KPC (3). However, the frequency and clinical relevance of ceftazidime-avibactam resistance in *Enterobacter* spp. are still unclear.

Cefiderocol is a novel catechol-substituted siderophore cephalosporin that has been

Citation Kawai A, McElheny CL, Iovleva A, Kline EG, Sluis-Cremer N, Shields RK, Doi Y. 2020. Structural basis of reduced susceptibility to ceftazidime-avibactam and cefiderocol in *Enterobacter cloacae* due to AmpC R2 loop deletion. Antimicrob Agents Chemother 64:e00198-20. https://doi.org/10.1128/AAC.00198-20.

Address correspondence to Yohei Doi, yod4@pitt.edu.

Received 28 January 2020
Returned for modification 25 February 2020
Accepted 4 April 2020
Accepted manuscript posted online 13 April 2020
Published 23 June 2020

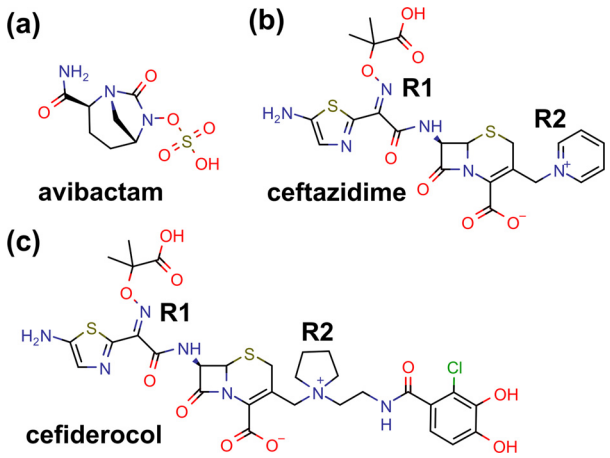

FIG 1 Chemical structures of avibactam (a), ceftazidime (b), and cefiderocol (c). The R1 and R2 side chains of cephalosporin are labeled. This figure was prepared by using MarvinSketch 19.20 (2019; ChemAxon).

approved for the treatment of complicated urinary tract infection in patients who have limited or no alternative treatment options (Fig. 1c) (4). Cefiderocol is actively transported across the Gram-negative outer membrane into the periplasmic space due to the halogenated catechol moiety on the C-3 side chain that chelates ferric ion and binds primarily to PBP3 (5). It is stable against all classes of β-lactamases, including metallo-β-lactamases, owing to the presence of the cyclic quaternary ammonium moiety on the same side chain. Thanks to these unique structural modifications, cefiderocol demonstrates potent activity across Gram-negative bacterial species, including carbapenem-resistant *Enterobacter* spp. In a surveillance of more than 9,000 contemporary clinical strains from North America and Europe, the MICs of cefiderocol were $\leq$4 μg/ml (the susceptibility breakpoint endorsed by the Clinical and Laboratory Standards Institute [CLSI]) for 99.9% of *Enterobacterales* clinical strains, 99.9% of *P. aeruginosa* strains, 97.6% of *A. baumannii* strains, 100% of *S. maltophilia* strains, and 93.8% of *Burkholderia cepacia* strains (6). More recently, the U.S. Food and Drug Administration has approved a susceptibility breakpoint of 2 μg/ml for *Enterobacterales*. For the 214 *E. cloacae* isolates tested in this surveillance study, the cefiderocol MIC_{90} was 1 μg/ml, with MICs ranging between 0.008 and 128 μg/ml. The mechanisms underlying resistance in isolates with high MICs have not been elucidated.

Here, we report the genetic, biochemical, and structural characterization of a variant AmpC identified in an *E. cloacae* clinical strain resistant to both ceftazidime-avibactam and cefiderocol.

RESULTS AND DISCUSSION

***E. cloacae* strain with reduced susceptibility to meropenem, ceftazidime-avibactam, and cefiderocol.** *E. cloacae* Ent385 was isolated from a patient who had undergone small-bowel transplant and presented to a hospital in Pennsylvania for fever, vomiting, abdominal pain, and distention. The patient received courses of meropenem and piperacillin-tazobactam, but not cephalosporins. On hospital day 30, the patient developed ventilator-associated pneumonia that was empirically treated with meropenem. A diagnostic bronchoalveolar lavage culture grew carbapenem-resistant *E. cloacae* (Ent385) with meropenem and ceftazidime-avibactam MICs of 16 and 8 μg/ml, respectively. Given the concerning susceptibility pattern, the strain was subjected to MIC testing of cefiderocol. The cefiderocol MIC of *E. cloacae* Ent385 was $>$16 μg/ml, which was unusually high and interpreted as resistant according to the provisional susceptibility breakpoint provided by the Clinical and Laboratory Standards Institute (CLSI; $\leq$4 μg/ml). By whole-genome sequencing, the strain belonged to sequence type (ST) 456 and carried bla_{DHA-1}, bla_{OXA-1}, and bla_{TEM-1} acquired β-lactamase genes, in addition to intrinsic *ampC*. DHA-1 is an acquired AmpC

TABLE 1 β-Lactam MICs against clinical and laboratory-generated strains with or without variant AmpC

Strain	AmpC variant	MIC (μg/ml)[a]									
		CAZ	CZA	FDC	FEP	MEM	IPM	MVB	I-R	ATM	ATA
E. cloacae Ent385	A294_P295del	>512	8	>16	128	16	16	16	4	>128	8
E. coli TOP10(pAmpC^{Ent385})	A294_P295del	256	2	2	4	≤0.06	0.5	0.03	0.25	16	0.25
E. coli TOP10(pAmpC^{Ent385Rev})	Wild type	128	0.5	0.5	0.25	≤0.06	0.5	0.03	0.25	16	0.25
E. coli TOP10(pBCSK(–))	Vector control	0.5	≤0.25	≤0.03	≤0.25	≤0.06	0.25	0.03	0.25	0.25	≤0.125

[a]CAZ, ceftazidime; CZA, ceftazidime-avibactam; FDC, cefiderocol; FEP, cefepime; MEM, meropenem; IPM, imipenem; MVB, meropenem-vaborbactam; I-R, imipenem-relebactam; ATM, aztreonam; ATA, aztreonam-avibactam.

β-lactamase that is nearly identical to the intrinsic AmpC of *Morganella morganii* (7). The ceftazidime-avibactam MIC_{90} against clinical isolates that produce DHA-1 is 0.5 μg/ml (8). OXA-1 and TEM-1 are an oxacillinase and a penicillinase, respectively, and confer resistance to penicillins. While no carbapenemase gene was identified, *ompC* and *ompF* possessed nonsynonymous mutations that corresponded to loss of the start codon (Met→Arg) and an early stop codon at position 66 (Ser→Stop), respectively. Functional loss of these two major outer membrane protein genes, coupled with production of DHA-1, likely accounted for meropenem resistance of *E. cloacae* Ent385 (9, 10). These mutations may have resulted from the patient's previous exposure to meropenem, but none of the prior cultures grew *E. cloacae*; thus, we could not examine this possibility.

AmpC R2 loop deletion as the source of reduced ceftazidime-avibactam and cefiderocol susceptibility in *E. cloacae* Ent385. The whole-genome sequencing of *E. cloacae* Ent385 identified an alanine-proline deletion at positions 294 and 295 (A294_P295del) and a leucine-to-valine substitution at position 296 (L296V) in the *ampC* gene. Various insertions, deletions, and amino acid substitutions in the H-10 helix or the R2 loop of *ampC* in various *Enterobacterales* and *P. aeruginosa* clinical strains have previously been associated with extension of the spectrum of hydrolysis to include cefepime, which is usually resistant to hydrolysis (11–17). We therefore hypothesized that A294_P295del observed in *ampC* might be the source of reduced susceptibility to cefiderocol and possibly also ceftazidime-avibactam.

To exclude the involvement of novel β-lactamases that had not been previously characterized or not catalogued in ResFinder, we conducted functional genome cloning of *E. cloacae* Ent385 using ampicillin resistance as the marker for β-lactamase production. As a result, several *E. coli* TOP10 transformants harboring recombinant pBCSK(–) plasmids were obtained. They all showed reduced susceptibility to ceftazidime-avibactam and cefiderocol compared to empty vector control. The recombinant plasmid with the shortest inserted fragment of ~2.3 kb (pAmpC^{Ent385}) containing part of *ampR* and the entire *ampC* was used for subsequent experiments.

Ceftazidime-avibactam and cefiderocol MICs of *E. coli* TOP10(pAmpC^{Ent385}) were both 2 μg/ml. The corresponding MICs of *E. coli* TOP10(pAmpC^{Ent385Rev}), in which A294_P295del was reverted to wild type by site-directed mutagenesis, were both 0.5 μg/ml (Table 1). These results confirmed the contribution of this R2 loop deletion to the ceftazidime-avibactam and cefiderocol-resistant phenotype in *E. cloacae* Ent385. The higher cefiderocol MIC of the parental *E. cloacae* strain may be further augmented by increased expression of pAmpC^{Ent385}.

AmpC^{Ent385} shows augmented hydrolysis of ceftazidime and cefiderocol. To further define the altered kinetic properties imparted by A294_P295del, AmpC^{Ent385} and AmpC^{Ent385Rev} were purified and subjected to measurements of the steady-state kinetic parameters k_{cat} and K_m for nitrocefin, cephalothin, ceftazidime, and cefiderocol (Table 2). Compared to AmpC^{Ent385Rev}, AmpC^{Ent385} showed substantial (~5-fold) reduction in k_{cat} values for nitrocefin and cephalothin, while the K_m values were within a 2-fold difference. This resulted in overall lower hydrolytic efficiency of AmpC^{Ent385} for these substrates. For ceftazidime, however, k_{cat} was significantly higher with AmpC^{Ent385} in comparison with AmpC^{Ent385Rev}, yielding an ~1,000-fold higher hydrolytic

TABLE 2 Kinetic parameters of AmpC^{Ent385} and AmpC^{Ent385Rev}

Substrate	AmpC^{Ent385}			AmpC^{Ent385Rev}			$(k_{cat}/K_m)^{Ent385}/(k_{cat}/K_m)^{Ent385Rev}$
	k_{cat} (s^{-1})	K_m (μM)	k_{cat}/K_m (μM^{-1} s^{-1})	k_{cat} (s^{-1})	K_m (μM)	k_{cat}/K_m (μM^{-1} s^{-1})	
Nitrocefin	18.4 ± 1.8	11.0 ± 4.7	1.67	92.6 ± 8.1	21.1 ± 3.6	4.39	0.38
Cephalothin	73.1 ± 9.9	0.34 ± 0.12	215	432 ± 150	0.17 ± 0.10	2,540	0.85×10^{-1}
Ceftazidime	25.8 ± 3.8	49.0 ± 25.2	0.53	$(0.30 \pm 0.07) \times 10^{-1}$	80.0 ± 29.6	0.38×10^{-3}	1,394.7
Cefiderocol	0.14 ± 0.03	49.8 ± 8.6	0.28×10^{-2}	0.08 ± 0.02	533 ± 267	0.15×10^{-3}	18.6

efficiency. For cefiderocol, the difference was with the affinity, with AmpC^{Ent385} showing 10-fold lower K_m, whereas the k_{cat} values were comparable. Overall for cefiderocol, this resulted in an ~20-fold higher hydrolytic efficiency with AmpC^{Ent385} compared to AmpC^{Ent385Rev}. The kinetic studies indicated that AmpC^{Ent385} shows a broad substrate specificity, including cefiderocol, and superior hydrolysis of ceftazidime, whereas its catalytic property against more classic cephalosporin substrates is slightly inferior to the native AmpC. The 50% inhibitory concentrations (IC_{50}s) of avibactam, measured using nitrocefin as the reporter substrate, were 0.04 ± 0.04 μM and 0.08 ± 0.02 μM, respectively, for AmpC^{Ent385} and AmpC^{Ent385Rev}, demonstrating that the potencies of inhibition by avibactam are almost identical. Thus, we speculate that the enhanced hydrolytic efficiency of ceftazidime primarily contributes to the reduced ceftazidime-avibactam susceptibility exhibited by AmpC^{Ent385}.

The overall structure of AmpC^{Ent385} indicates a local structural change of the R2 loop. To obtain further structural insights on AmpC^{Ent385} showing superior catalytic properties against ceftazidime and cefiderocol, we determined crystal structures of the AmpC^{Ent385} free form and its complexes with ceftazidime or avibactam (referred to as the AmpC^{Ent385}-CAZ complex and the AmpC^{Ent385}-AVI complex, respectively). The data collection and refinement statistics are summarized in Table 3. The AmpC^{Ent385} crystal belongs to the space group $P2_1$, and there are two AmpC^{Ent385} monomers contained in a crystallographic asymmetric unit. The qualities of the electron density maps were better for chain A in common to the AmpC^{Ent385} structures, and almost all residues except for the C-terminal Q259 residue could be assigned in the chain A structures. On the other hand, several disordered regions were observed in chain B of the AmpC^{Ent385} structures, and we could not model the following structures: residues of P140 to A143 (P140–A143) and N289–P295 for the free form; residues of T113–N128, P140–A151, and D279–P295 for the AmpC^{Ent385}-CAZ complex; and residues of T111–Q120, Q139–A151, and V280–P295 for the AmpC^{Ent385}-AVI complex. Thus, we describe the following results and discussion of the AmpC^{Ent385} structures based on the chain A structures.

According to the previous structural studies, the overall fold of class C β-lactamase consists of an α-helical domain and a mixed α/β domain, and the active site is located between the two domains (18). AmpC^{Ent385} also has a typical fold of class C β-lactamase (Fig. 2a). The overall structure of the AmpC^{Ent385} free form is quite similar to those of the AmpC^{Ent385}–CAZ complex and the AmpC^{Ent385}–AVI complex, with 0.16 Å and 0.18 Å of the root mean square deviation (RMSD) values for the corresponding Cα positions for 356 residues, respectively (Fig. 2a). These results suggest that AmpC^{Ent385} does not require an overall structural change for substrate recognition. Electron density maps corresponding to the molecules of ceftazidime and avibactam were observed in the active site of each AmpC^{Ent385}-drug complex structure. These electron density maps were continuously extended to the catalytic residue S64 of AmpC^{Ent385}, indicating that Oγ atom of S64 is covalently bound to C-8 atom of ceftazidime or the C-7 atom of avibactam, and these structures displayed acyl-enzyme intermediates of the AmpC^{Ent385}-drug complex structures (Fig. 2b and c). The R1 side chain of cefiderocol is identical to that of ceftazidime (Fig. 1b and c). The R2 side chain of cefiderocol is a bulkier pyrrolidine group with the catechol moiety, while that of ceftazidime is a pyridinium group. However, these R2 side chain are liberated during the hydrolysis reaction (19). Thus, we hypothesize that the final AmpC^{Ent385} acyl-complex structure with cefiderocol is identical to the AmpC^{Ent385}-CAZ complex structure.

TABLE 3 Data collection and structure refinement statistics[a]

Data set	Free form	AVI complex	CAZ complex
Data collection			
Source	Photon Factory BL-17A	Photon Factory BL-17A	Photon Factory BL-17A
Wavelength (Å)	0.9800	0.9800	0.9800
Space group	$P2_1$	$P2_1$	$P2_1$
Unit cell parameters			
Length (Å)	$a = 50.6$, $b = 75.2$, $c = 103.4$	$a = 50.4$, $b = 73.7$, $c = 102.1$	$a = 50.4$, $b = 74.1$, $c = 102.3$
Angle (°)	$\beta = 95.1$	$\beta = 94.5$	$\beta = 94.8$
Resolution range (Å)	46.9–1.40 (1.48–1.40)	46.5–1.60 (1.70–1.60)	46.7–1.65 (1.75–1.65)
No. of observed reflections	1,039,223 (169,454)	668,610 (109,167)	630,466 (100,564)
No. of unique reflections	149,918 (23,824)	96,869 (15,241)	89,346 (14,132)
Multiplicity	6.9 (7.1)	6.9 (7.2)	7.1 (7.1)
Completeness (%)	98.7 (97.2)	98.4 (96.3)	98.1 (96.6)
R_{merge} (%)[b]	4.9 (66.0)	5.9 (66.6)	5.7 (77.3)
$\langle I/\sigma\ (I)\rangle$	18.66 (2.59)	16.86 (2.45)	18.84 (2.35)
Refinement			
Resolution (Å)	46.9–1.40 (1.42–1.40)	37.6–1.60 (1.62–1.60)	43.7–1.65 (1.67–1.65)
No. of reflections used	149,881 (4,852)	96,856 (2,991)	89,321 (2,904)
R_{work} (%)[c]	14.7 (23.1)	16.7 (23.6)	16.3 (29.9)
R_{free} (%)[d]	16.8 (25.5)	18.9 (23.3)	19.4 (36.8)
No. of nonhydrogen atoms	6,613	6,059	6,003
Protein	5,811	5,342	5,281
Ligands	110	113	122
Solvent	696	604	600
RMSD from ideality			
Bond length (Å)	0.004	0.005	0.009
Bond angle (°)	0.763	0.775	0.928
Avg B-factor	24.8	29.5	29.4
Protein	22.8	27.9	27.8
Ligands	54.6	56.1	48.8
Solvent	37.4	39.0	39.8
Ramachandran plot			
Favored region (%)	98.85	98.80	98.63
Allowed region (%)	1.15	1.20	1.37
Outlier region (%)	0.00	0.00	0.00
Clashscore	2.12	2.22	1.40
PDB ID	6LC7	6LC8	6LC9

[a]Values in parentheses denote the highest-resolution shell.
[b]$R_{merge} = 100 \times \Sigma_{hkl} \Sigma_i |I_i(hkl) - \langle I(hkl)\rangle| / \Sigma_{hkl} \Sigma_i I_i(hkl)$, where $\langle I(hkl)\rangle$ is the mean value of $I(hkl)$.
[c]$R_{work} = 100 \times \Sigma_{hkl} ||F_o| - |F_c|| / \Sigma_{hkl} |F_o|$, where F_o and F_c the observed and calculated structure factors, respectively.
[d]R_{free} is calculated as for R_{work}, but for the test set comprising 5% reflections not used in refinement.

To clarify the structural changes of AmpC^{Ent385} due to A294_P295del, the crystal structure of AmpC^{Ent385} was superimposed on the crystal structure of AmpC P99 isolated from *Enterobacter hormaechei* (referred to as AmpC^{P99}, PDB ID 5XHR) (20), having 84% sequence identity over 359 residues. As a result, a structural difference between AmpC^{Ent385} and AmpC^{P99} was observed in V283–V294 residues of AmpC^{Ent385}, and the RMSD value for the corresponding Cα positions of this region is over at least 1 Å, while the overall RMSD value for the corresponding Cα positions for 351 residues is 0.65 Å. In detail, relative to the AmpC^{P99} structure, H-9 helix of AmpC^{Ent385} is slightly slanted (Fig. 3). The Cα positions of S287 located at the C-terminal side of H-9 helix shift 3.3 Å, and the Cα position of S287 of AmpC^{Ent385} and that of AmpC^{P99} subtends approximately 15° from the Cα position of D279 of AmpC^{Ent385}. Slanted H-9 helix is directly connected with the R2 loop, and the H-10 helix disappears in the AmpC^{Ent385} structure.

Structural changes of AmpC^{Ent385} account for its altered kinetic properties. The active site of the AmpC^{Ent385}-CAZ complex is shown in Fig. 4. A total of 12 hydrogen bonds were observed in the AmpC^{Ent385}-CAZ complex, and AmpC^{Ent385} recognizes ceftazidime by a tight hydrogen bond network in a manner that is similar to ceftazidime recognition by the native AmpC isolated from *E. coli* (referred to as AmpC^{Ec}, having 73% sequence identity over 356 residues with AmpC^{Ent385}, PDB ID 1IEL; Fig. 4a) (21). The

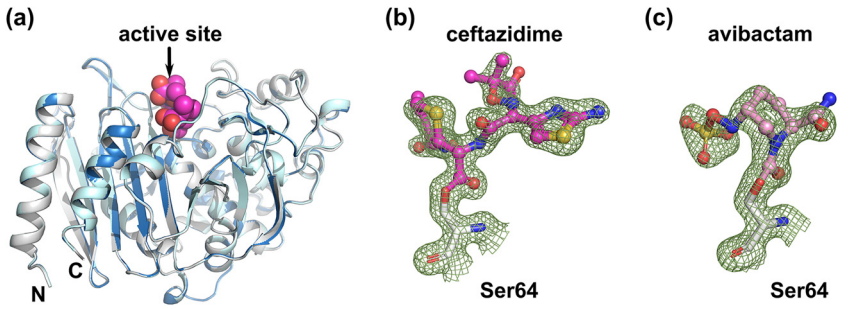

FIG 2 Overall structures of AmpC^{Ent385}. (a) The AmpC^{Ent385} structures are shown as cartoon representations and colored white for the AmpC^{Ent385} free form, blue for the AmpC^{Ent385}-CAZ complex, and cyan for the AmpC^{Ent385}-AVI complex. To indicate the active site, the ceftazidime molecule is shown as CPK (space-filling model) representation colored magenta. (b and c) 2mF_o-DF_c maps are shown as green mesh contoured 1.5σ. The molecules of ceftazidime and avibactam are shown as ball-and-stick representations colored magenta and pink, respectively.

carbonyl oxygen atom of the ester bond between AmpC^{Ent385} and ceftazidime forms hydrogen bonds to main chain nitrogen atoms of S64 and S316. The C4 carboxyl group of the dihydrothiazine ring of ceftazidime forms hydrogen bonds to side chains of N289 and N344 and two water molecules. The amide group at the R1 side chain of ceftazidime forms hydrogen bonds to side chains of Q120 and N152. The carboxyl group and the aminothiazole ring at the R1 side chain of ceftazidime form hydrogen bonds to one and two water molecules, respectively. The deacylating water molecule, which is predicted by the AmpC^{Ec} structure, was observed in the AmpC^{Ent385}–CAZ complex structure, and its position and interaction with AmpC^{Ent385} were similar to those of AmpC^{Ec} (Fig. 4b). In the native AmpC^{Ec}-CAZ complex structure, the position of the R2 side chain (R2 site) is surrounded by the R2 loop, including the H-10 helix (Fig. 4d).

Figure 5 shows the active site of the AmpC^{Ent385}-AVI complex. AmpC^{Ent385} recognizes avibactam through several hydrogen bonds that also recognize ceftazidime. The carbonyl oxygen atom of the ester bond between S64 of AmpC^{Ent385} and avibactam forms hydrogen bonds to main chain nitrogen atoms of S64 and S316. The carboxamide group of piperidine ring of avibactam forms hydrogen bonds to side chains of Q120 and N152. The sulfate group of avibactam forms hydrogen bonds to side chains of N289, K313, T314, and N344, main chain oxygen atom of T314 and one water molecule. To date, the following four crystal structures of the class C β-lactamase complex with avibactam have been reported: PDC-1 (PDB ID 4OOY and 4HEF) (22, 23), FOX-4 (PDB ID 5ZA2) (24), and TRU-1 (PDB ID 6FM7) (25). Comparison of the AmpC^{Ent385}-AVI complex structure with the other structures of class C β-lactamase complex with avibactam indicates that the hydrogen bond between N289 of AmpC^{Ent385} and the sulfate group of avibactam is an interaction unique to the AmpC^{Ent385}-AVI complex, while the rest of the hydrogen bond network involved in the recognition of avibactam is similar (Fig. 5b). This unique interaction could be attributed to the translocation of N289 due to

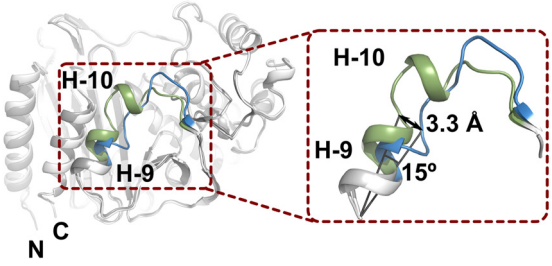

FIG 3 Structure comparison of AmpC^{Ent385} and AmpC^{P99}. The structures of AmpC^{Ent385} and AmpC^{P99} are shown as cartoon representations and colored white and gray, respectively. To clarify the difference, the colors of the V283–V294 residue structures in AmpC^{Ent385} and the corresponding residues in AmpC^{P99} appear in blue and green, respectively.

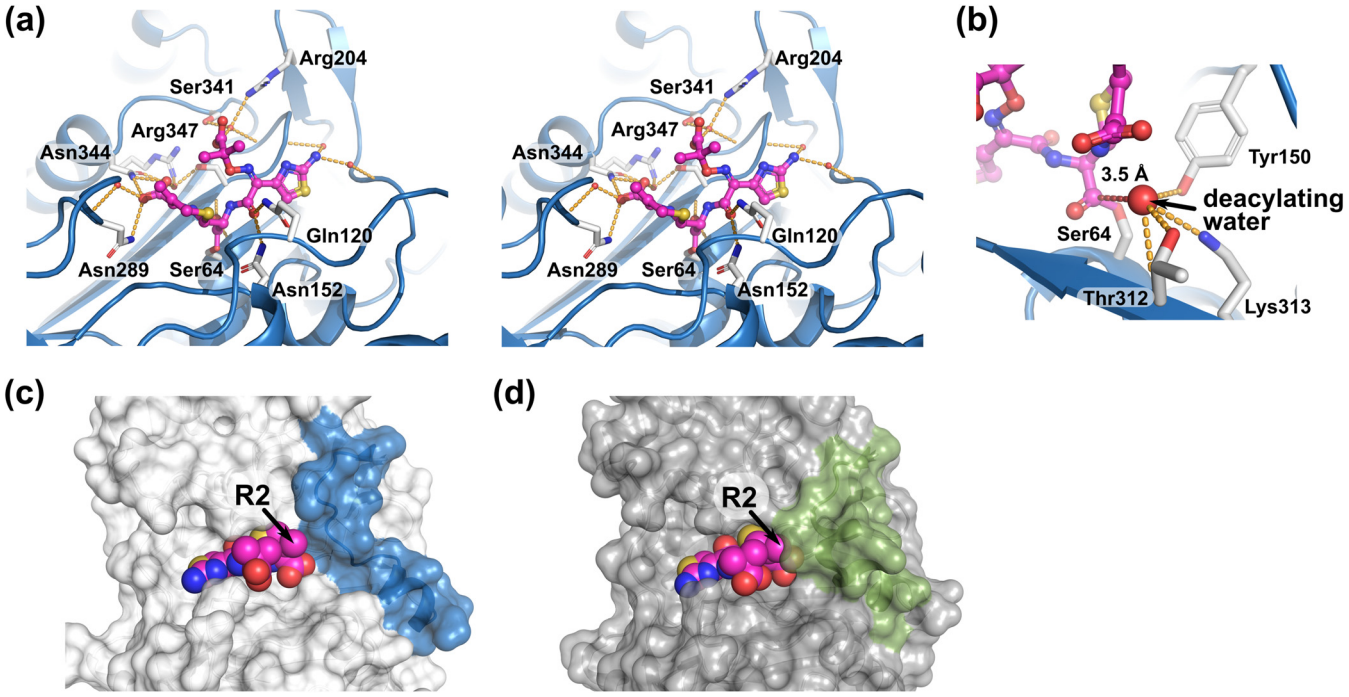

FIG 4 Ceftazidime recognition by AmpC^{Ent385}. (a) Stereo view of the ceftazidime binding. The ceftazidime molecule as shown in ball-and-stick representations colored magenta. Hydrogen bonds are shown as orange dashed lines. Residues and the water molecules participating the hydrogen bond network are shown as white stick and red spheres, respectively. (b) The deacylating water molecule is shown as a large red sphere. Red dashed line indicates the distance between C-8 atom of ceftazidime and the deacylating water molecule. (c and d) Comparison of the substrate-binding sites of the AmpC^{Ent385}-CAZ complex and the AmpC^{Ec}-CAZ complex. Transparent molecular surfaces of AmpC^{Ent385} (c) and AmpC^{Ec} (d) are colored white and gray, respectively. To clarify the difference, the colors of the V283–V294 residue structures, including R2 loop in AmpC^{Ent385}, and corresponding residues in AmpC^{P99} appear in blue and green, respectively. Arrowheads indicate the R2 side chain positions of ceftazidime.

A294_P295del. In addition, the AmpC^{Ent385}-AVI complex structure shows that the sulfate group of avibactam bound to AmpC^{Ent385} at the R2 site is exposed due to the disappearance of H-10 helix (Fig. 5c and d).

These structural studies of AmpC^{Ent385} revealed that A294_P295del induces local structural change from the H-9 helix to the R2 loop and the disappearance of the H-10 helix (Fig. 3), while the hydrogen bond network between AmpC^{Ent385} and ceftazidime or avibactam and the key residues of AmpC^{Ent385} involved in the reaction are largely conserved compared to that of the native AmpC (Fig. 4 and 5). The results indicated that the structural change in AmpC^{Ent385} enables extension of the substrate-binding site to the bulk solvent region and recognition of cephalosporins having bulkier R2 side chains such as cefiderocol, thus allowing for relevant levels of hydrolysis to occur (Fig. 4c). Cefiderocol will escape recognition by the native AmpC due to the steric hindrance between the bulkier R2 side chain of cefiderocol and the R2 site of the native AmpC, which conceals this binding site with the H-10 helix (Fig. 1c and 4d). These observations are consistent with the results of the kinetic studies showing ~10-fold lower K_m of AmpC^{Ent385} for cefiderocol compared to AmpC^{Ent385Rev} (Table 2). With cefiderocol, the substrate-binding to the active site may be essential for the occurrence of relevant levels of hydrolysis. In addition, the kinetic parameters show that ceftazidime is a better substrate for AmpC^{Ent385} (Table 2). Ceftazidime has a smaller R2 side chain than that of cefiderocol (Fig. 1b and c), and it is well known that the native AmpC modestly hydrolyzes ceftazidime, indicating that its binding to the native AmpC is sufficient for relevant levels of ceftazidime hydrolysis to occur. We speculate that expansion of the substrate-binding site of AmpC^{Ent385} also increases the rates of both the substrate binding and the product leaving of ceftazidime, resulting in improved turnover of ceftazidime, whereas the substrate affinity is largely maintained.

Genetic changes (deletions, insertions, and amino acid substitutions) in the R2 site of AmpC have historically been associated with extension of the AmpC substrate

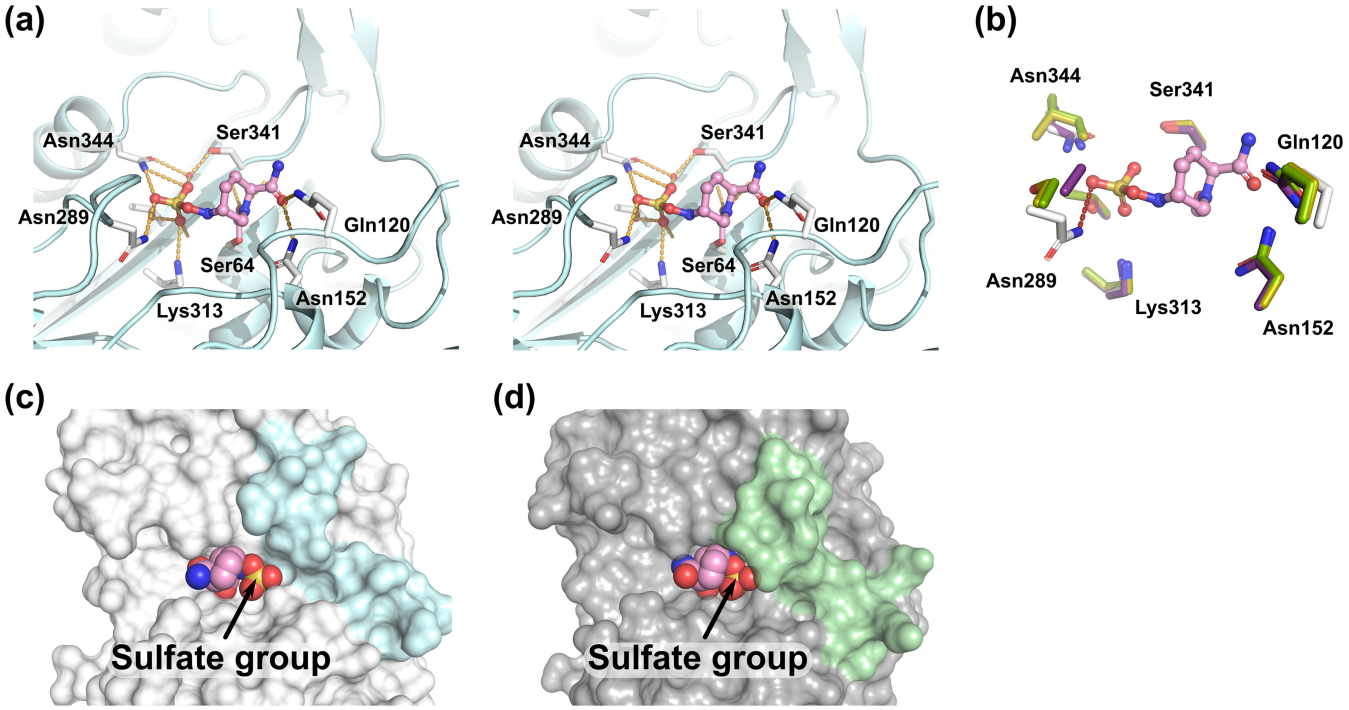

FIG 5 Avibactam recognition by AmpC^{Ent385}. (a) Stereo view of the avibactam binding. The avibactam molecule is shown as ball-and-stick representations colored pink. Hydrogen bonds are shown as orange dashed lines. Residues and the water molecules participating the hydrogen bond network are shown as white stick and red spheres, respectively. (b) Structure comparisons of the AmpC^{Ent385}-AVI complex to the other class C β-lactamase complex with avibactam. Colors are white for AmpC^{E385}, purple for PDC-1 (PDB ID 4OOY), green for FOX-4 (PDB ID 5ZA2), and yellow for TRU-1 (PDB ID 6FM7). Red dashed line indicates a unique hydrogen bond between N289 of AmpC^{Ent385} and the sulfate group of avibactam. Residues of AmpC^{Ent385} are labeled. (c and d) Comparison of the substrate-binding sites of the AmpC^{Ent385}-AVI complex and the PDC-1–AVI complex (PDB ID 4OOY). Transparent molecular surfaces of AmpC^{Ent385} (c) and PDC-1 (d) are colored in white and gray, respectively. To clarify the difference, the colors of the V283–V294 residue structures, including the R2 loop in AmpC^{Ent385}, and corresponding residues in PDC-1 appear in cyan and pale green, respectively. Arrowheads indicate the sulfate group of avibactam.

specificity to cefepime in several species, including *E. cloacae*, *Klebsiella aerogenes*, *Serratia marcescens*, *Citrobacter freundii*, *E. coli* and *Pseudomonas aeruginosa* (11–18). Crystal structures of AmpC, including these genetic changes in the R2 site, were reported on AmpC^{D} (containing three amino acid deletions at positions 286 to 288, PDB ID 2ZJ9) (26) and AmpC BER (containing two alanine residues insertions at positions 294 and 295, PDB ID 5JOC) (27), and these structures show similar local structural changes at the R2 site observed in the AmpC^{Ent385} structure. Although it is not known whether these previously reported variant AmpCs also confer reduced susceptibility to ceftazidime-avibactam and/or cefiderocol, this suggests that similar variants may arise in species other than *E. cloacae* as reported here.

Conclusion. There continues to be a need for new therapeutics to treat highly drug-resistant Gram-negative bacterial infections. Ceftazidime-avibactam has been successfully used in the treatment of carbapenem-resistant *Enterobacterales* infection in regions where KPC is the predominant carbapenemase type. Cefiderocol, a novel siderophore cephalosporin, possesses broad-spectrum activity against Gram-negative pathogens. Based on microbiological surveillance studies, cefiderocol maintains potency across Gram-negative bacterial species of clinical relevance, regardless of the β-lactamase background (6, 28, 29). From a clinical standpoint, cefiderocol is notably active against most carbapenem-resistant *Enterobacterales* strains, including those producing KPC, NDM, and OXA-48-group carbapenemases. While isolates resistant to cefiderocol have been rarely identified in surveillance studies, the underlying mechanisms have not been reported. Here, we demonstrated that a two amino acid deletion in the R2 loop of AmpC β-lactamases can confer reduced susceptibility to ceftazidime-avibactam and cefiderocol, which can be attributed to the drastic structural changes of the H-9 and H-10 helices and the R2 loop induced by the deletion and consequent

increased hydrolysis of ceftazidime and cefiderocol. The findings provide new insights into how multidrug-resistant Gram-negative bacteria might evolve their β-lactamases to survive selective pressure from the latest β-lactam agents that are engineered to combat them.

MATERIALS AND METHODS

Strains and plasmids. *E. cloacae* Ent385 was a clinical strain isolated from the respiratory tract of a hospitalized patient. The isolate was initially identified as *E. cloacae* complex by using a matrix-assisted laser desorption ionization--time of flight approach and later confirmed to belong to *E. cloacae* species as described below. *E. coli* TOP10 and cloning vector pBCSK(–) were used for initial cloning of the ceftazidime-avibactam and cefiderocol resistance determinant. *E. coli* BL21(DE3) and expression vector pET30b were used for purification of AmpC^{Ent385} and AmpC^{Ent385Rev} (revertant of the R2 loop deletion in AmpC^{Ent385}).

Whole-genome sequencing. The genome of strain Ent385 was sequenced by Illumina NextSeq using a paired-end protocol. The reads were assembled into contigs by CLC Genomics Workbench 11. The species was confirmed with the average nucleotide identity method, and the sequence type was determined *in silico* (https://pubmlst.org/ecloacae/). Antimicrobial resistance genes were identified by ResFinder version 3.2 (https://cge.cbs.dtu.dk/services/ResFinder/).

Cloning and sequencing of AmpC^{Ent385}. The cefiderocol resistance determinant was sought by shotgun cloning of the *E. cloacae* Ent385 genome. In brief, genomic DNA was extracted, purified. and partially digested with Sau3AI, which was then ligated with BamHI-digested pBCSK(–). *E. coli* TOP10 was transformed with the ligated products, and transformants were selected by growth on lysogenic broth agar containing 50 μg/ml of ampicillin. The recombinant plasmids were sequenced on both strands by Sanger sequencing.

Susceptibility testing. MICs of *E. cloacae* Ent385 and *E. coli* producing AmpC^{Ent385} were obtained by standard broth microdilution methods. For cefiderocol, iron-depleted cation-adjusted Mueller-Hinton broth plates provided by Shionogi, Inc., through International Health Management Associates (Schaumburg, IL) were used to test susceptibility (30).

Generation of AmpC^{Ent385Rev}. AmpC^{Ent385Rev} was generated by site-directed mutagenesis according to the manufacturer's protocol of the Q5 site-directed mutagenesis kit (New England Biolabs, Ipswich, MA). Briefly, engineered forward (5′-CGCCGTTGCCGGTCGCAGAAGTGA-3′) and reverse (CCAGTGCGACC TTATTGTCG) primers including the six deleted nucleotides were used to amplify AmpC^{Ent385}. The PCR system contained 10 ng template, 2× Q5 Hot Start High-Fidelity Master Mix, and 0.5 μM concentrations of each primer in a total volume of 25 μl. The PCR began with an initial denaturation at 98°C (30 s), followed by 25 cycles at 98°C for 10 s, 60°C for 30 s, and 72°C for 1 min 45 s and then an extension step at 72°C for 7 min. The product (*ampC*^{Ent385Rev}) was sequenced to confirm addition of the six nucleotides. *ampC*^{Ent385} and *ampC*^{Ent385Rev} were subcloned into pET30b using NdeI and EcoRI and transferred into the *E. coli* BL21(DE3) strain.

Purification of AmpC^{Ent385} and AmpC^{Ent385Rev} for kinetic measurements. Lysogenic broth plus kanamycin (50 μg/ml) was inoculated with *E. coli* BL21(DE3) harboring the pET30b-AmpC^{Ent385} or pET30b-AmpC^{Ent385Rev} recombinant plasmids and grown to an optical density at 600 nm of 0.5 to 0.7. A final concentration of 0.1 mM IPTG (isopropyl-β-D-thiogalactopyranoside) was added, and the culture was incubated for an additional 2 h. The cells were harvested by centrifugation; the pellet was then resuspended in 20 mM Tris-HCl (pH 7.0) buffer, sonicated, and centrifuged at 8,000 rpm for 10 min at 4°C to remove cell debris. The supernatants, containing the active enzymes, were ultracentrifuged at 100,000 × *g* and filtered through a 0.45 μm Durapore membrane filter (Millipore, Billerica, MA). The crude extract was loaded onto a HiTrap SP HP (GE Healthcare) previously equilibrated with 20 mM Tris-HCl (pH 7.0). The AmpC enzymes were then eluted with a NaCl gradient at a flow rate of 5 ml/min. Fractions containing active enzyme were pooled, concentrated, and dialyzed into PBS (pH 7.2) using an Amicon Ultra spin column with a cut off size of 10 kDa (Millipore) to yield salt-free enzymes approximately 10 mg in quantity and >95% in purity as determined by SDS-PAGE.

Kinetic measurements. The steady-state kinetic parameters were determined in phosphate-buffered saline (PBS; pH 7.2) with a constant amount of enzyme and various concentrations of the substrates using a UV spectrophotometer (V-750; JASCO, Easton, MD). Substrates tested included nitrocefin, cephalothin, ceftazidime, and cefiderocol. For avibactam, the concentration of avibactam which gave a 50% reduction in the hydrolysis of nitrocefin (IC_{50}) was measured after 5 min of preincubation of the enzyme with the inhibitor at 25°C (room temperature) and nitrocefin as the substrate at 100 μM. Three independent measurements were performed for each enzyme and substrate or inhibitor combination.

Purification of AmpC^{Ent385} for the X-ray crystallography. The gene encoding residues 21 to 379 of AmpC^{Ent385} without the signal peptide was cloned into the expression plasmid vector pET30b between the restriction enzyme sites of NdeI and EcoRI. Purification was conducted in the same manner as the proteins for kinetic measurements. In addition, further purification was performed with a HiTrap Blue HP column (GE Healthcare, Chicago, IL) chromatography, and the proteins were eluted with a linear gradient of 0 to 2 M NaCl in 20 mM Tris-HCl (pH 7.0). The purity of AmpC^{Ent385} was evaluated by SDS-PAGE analysis, and the β-lactamase activity was confirmed as described previously (31). The active fractions were collected and concentrated using a Vivaspin Turbo 4 centrifugal concentrator (MWCO 10,000; Sartorius, Gottingen, Germany), and the buffer was exchanged to 20 mM Tris-HCl (pH 7.0) by several

rounds of dilution and concentration. The purified active AmpC^{Ent385} solution was finally concentrated to 50 mg/ml and stored in 20 μl aliquots at −80°C until used in crystallization experiments.

Crystallization. Initial screening of AmpC^{Ent385} was performed with the commercial crystal screening kits Index, Crystal Screen, and Crystal Screen 2 (Hampton Research, Aliso Viejo, CA) using the hanging-drop vapor diffusion method by mixing 1.0 μl of the AmpC^{Ent385} solution (20 mg/ml) and 1.0 μl of the reservoir solution at 20°C. The cluster crystals of AmpC^{Ent385} appeared in no. 23 crystallization condition of Crystal Screen 2 kit within 2 months. Single crystals of AmpC^{Ent385} suitable for the X-ray crystallography were obtained by using the multiple rounds of streak-seeding methods with aforementioned cluster crystals, and the droplets were prepared by mixing 1.5 μl of the AmpC^{Ent385} solution (20 mg/ml) and 1.5 μl of the reservoir solution containing 1.8 M ammonium sulfate, 0.1 M MES (pH 5.5), and 5% 1,4-dioxane and were preequilibrated for 1 week at 4°C. Crystals of the AmpC^{Ent385}-CAZ complex and the AmpC^{Ent385}-AVI complex were obtained by soaking the AmpC^{Ent385} crystals in a solution containing 10 mM ceftazidime or 10 mM avibactam, 1.8 M ammonium sulfate, 0.1 M MES (pH 5.5), and 5% 1,4-dioxane at 4°C for 3 h.

Data collection, structure determination, and refinement. Prior to the X-ray experiments, the AmpC^{Ent385} crystals were transferred into a cryoprotectant solution composed of reservoir solution containing 30% glycerol and then flash frozen in liquid nitrogen. Synchrotron experiments were carried out using Photon Factory BL-17A (High Energy Accelerator Research Organization, Tsukuba, Japan). Diffraction data sets were collected at −173°C using an EIGER X16M detector, and data sets were processed and scaled using XDS (32). The initial phase of the AmpC^{Ent385} structure was determined by the molecular replacement method using Molrep (33) from the CCP4 program suite (34), with the coordinate (PDB ID 5XHR) serving as the search model (20). Manual model rebuilding was performed with COOT (35). Structure refinements were performed with phenix.refine from the PHENIX package (36). The AmpC^{Ent385} structure was refined with the anisotropic atomic displacement parameters. The structures of the AmpC^{Ent385}-CAZ complex and the AmpC^{Ent385}-AVI complex were refined with the atomic displacement parameters using the translation, liberation, and screw (TLS) method, and TLS groups were determined by using phenix.find_tls_groups. The stereochemical quality of the final structures were evaluated by MolProbity (37). All molecular graphics were prepared using PyMOL v2.3.2 (Schrödinger, New York, NY).

Data availability. The contigs of the *E. cloacae* Ent385 genome have been submitted to the NCBI under GenBank accession number WNXG00000000. The atomic coordinates of AmpC^{Ent385} have been submitted to the Protein Data Bank (PDB) under PDB accession numbers 6LC7 for the free form, 6LC8 for the complex with avibactam, and 6LC9 for the complex with ceftazidime.

ACKNOWLEDGMENTS

We thank Masahiro Suzuki for help in confirming the species of AmpC^{P99}-producing *Enterobacter cloacae* complex strain. Synchrotron experiments were performed with the approval of the Photon Factory Program Advisory Committee (proposal 2017G554). We are grateful to the beamline staff for their support of our synchrotron experiments and to Shionogi, Inc., for the provision of cefiderocol.

This study was supported by grant R21AI151362 from the National Institutes of Health. R.K.S. was supported by NIH grants K08AI114883 and R03AI144636. Y.D. was supported by NIH grants R01AI104895 and R21AI135522.

REFERENCES

1. Szabó D, Silveira F, Hujer AM, Bonomo RA, Hujer KM, Marsh JW, Bethel CR, Doi Y, Deeley K, Paterson DL. 2006. Outer membrane protein changes and efflux pump expression together may confer resistance to ertapenem in *Enterobacter cloacae*. Antimicrob Agents Chemother 50:2833–2835. https://doi.org/10.1128/AAC.01591-05.
2. van Duin D, Lok JJ, Earley M, Cober E, Richter SS, Perez F, Salata RA, Kalayjian RC, Watkins RR, Doi Y, Kaye KS, Fowler VG, Paterson DL, Bonomo RA, Evans S, Antibacterial Resistance Leadership Group. 2018. Colistin versus ceftazidime-avibactam in the treatment of infections due to carbapenem-resistant *Enterobacteriaceae*. Clin Infect Dis 66:163–171. https://doi.org/10.1093/cid/cix783.
3. Shields RK, Nguyen MH, Chen L, Press EG, Kreiswirth BN, Clancy CJ. 2018. Pneumonia and renal replacement therapy are risk factors for ceftazidime-avibactam treatment failures and resistance among patients with carbapenem-resistant *Enterobacteriaceae* infections. Antimicrob Agents Chemother 62:e02497-17. https://doi.org/10.1128/AAC.02497-17.
4. Food and Drug Administration. 2019. FDA news release. U.S. FDA, Bethesda, MD. https://www.fda.gov/news-events/press-announcements/fda-approves-new-antibacterial-drug-treat-complicated-urinary-tract-infections-part-ongoing-efforts. Accessed 19 November 2019.
5. Aoki T, Yoshizawa H, Yamawaki K, Yokoo K, Sato J, Hisakawa S, Hasegawa Y, Kusano H, Sano M, Sugimoto H, Nishitani Y, Sato T, Tsuji M, Nakamura R, Nishikawa T, Yamano Y. 2018. Cefiderocol (S-649266), A new siderophore cephalosporin exhibiting potent activities against *Pseudomonas aeruginosa* and other gram-negative pathogens including multidrug-resistant bacteria: structure activity relationship. Eur J Med Chem 155:847–868. https://doi.org/10.1016/j.ejmech.2018.06.014.
6. Karlowsky JA, Hackel MA, Tsuji M, Yamano Y, Echols R, Sahm DF. 2019. *In vitro* activity of cefiderocol, a siderophore cephalosporin, against Gram-negative bacilli isolated by clinical laboratories in North America and Europe in 2015–2016: SIDERO-WT-2015. Int J Antimicrob Agents 53:456–466. https://doi.org/10.1016/j.ijantimicag.2018.11.007.
7. Barnaud G, Arlet G, Verdet C, Gaillot O, Lagrange PH, Philippon A. 1998. *Salmonella enteritidis*: AmpC plasmid-mediated inducible β-lactamase (DHA-1) with an *ampR* gene from *Morganella morganii*. Antimicrob Agents Chemother 42:2352–2358. https://doi.org/10.1128/AAC.42.9.2352.
8. Karlowsky JA, Biedenbach DJ, Kazmierczak KM, Stone GG, Sahm DF. 2016. Activity of ceftazidime-avibactam against extended-spectrum- and AmpC β-lactamase-producing *Enterobacteriaceae* collected in the INFORM Global Surveillance Study from 2012 to 2014. Antimicrob Agents Chemother 60:2849–2857. https://doi.org/10.1128/AAC.02286-15.
9. Chen YG, Zhang Y, Yu YS, Qu TT, Wei ZQ, Shen P, Li LJ. 2008. *In vivo* development of carbapenem resistance in clinical isolates of *Enterobac-*

ter aerogenes producing multiple β-lactamases. Int J Antimicrob Agents 32:302–307. https://doi.org/10.1016/j.ijantimicag.2008.02.014.
10. Lee K, Yong D, Choi YS, Yum JH, Kim JM, Woodford N, Livermore DM, Chong Y. 2007. Reduced imipenem susceptibility in *Klebsiella pneumoniae* clinical isolates with plasmid-mediated CMY-2 and DHA-1 β-lactamases co-mediated by porin loss. Int J Antimicrob Agents 29:201–206. https://doi.org/10.1016/j.ijantimicag.2006.09.006.
11. Barnaud G, Labia R, Raskine L, Sanson-Le Pors MJ, Philippon A, Arlet G. 2001. Extension of resistance to cefepime and cefpirome associated with a 6-amino-acid deletion in the H-10 helix of the cephalosporinase of an *Enterobacter cloacae* clinical isolate. FEMS Microbiol Lett 195:185–190. https://doi.org/10.1111/j.1574-6968.2001.tb10519.x.
12. Mammeri H, Poirel L, Bemer P, Drugeon H, Nordmann P. 2004. Resistance to cefepime and cefpirome due to a 4-amino-acid deletion in the chromosome-encoded AmpC β-lactamase of a *Serratia marcescens* clinical isolate. Antimicrob Agents Chemother 48:716–720. https://doi.org/10.1128/aac.48.3.716-720.2004.
13. Doi Y, Wachino J-i, Ishiguro M, Kurokawa H, Yamane K, Shibata N, Shibayama K, Yokoyama K, Kato H, Yagi T, Arakawa Y. 2004. Inhibitor-sensitive AmpC β-lactamase variant produced by an *Escherichia coli* clinical isolate resistant to oxyiminocephalosporins and cephamycins. Antimicrob Agents Chemother 48:2652–2658. https://doi.org/10.1128/AAC.48.7.2652-2658.2004.
14. Mammeri H, Poirel L, Nordmann P. 2007. Extension of the hydrolysis spectrum of AmpC β-lactamase of *Escherichia coli* due to amino acid insertion in the H-10 helix. J Antimicrob Chemother 60:490–494. https://doi.org/10.1093/jac/dkm227.
15. Ahmed AM, Shimamoto T. 2008. Emergence of a cefepime- and cefpirome-resistant *Citrobacter freundii* clinical isolate harbouring a novel chromosomally encoded AmpC β-lactamase, CMY-37. Int J Antimicrob Agents 32:256–261. https://doi.org/10.1016/j.ijantimicag.2008.04.019.
16. Rodríguez-Martínez JM, Fernández-Echauri P, Fernández-Cuenca F, Diaz de Alba P, Briales A, Pascual A. 2012. Genetic characterization of an extended-spectrum AmpC cephalosporinase with hydrolysing activity against fourth-generation cephalosporins in a clinical isolate of *Enterobacter aerogenes* selected *in vivo*. J Antimicrob Chemother 67:64–68. https://doi.org/10.1093/jac/dkr423.
17. Berrazeg M, Jeannot K, Ntsogo Enguéné VY, Broutin I, Loeffert S, Fournier D, Plésiat P. 2015. Mutations in β-lactamase AmpC increase resistance of *Pseudomonas aeruginosa* isolates to antipseudomonal cephalosporins. Antimicrob Agents Chemother 59:6248–6255. https://doi.org/10.1128/AAC.00825-15.
18. Powers RA. 2016. Structural and functional aspects of extended-spectrum AmpC cephalosporinases. Curr Drug Targets 17:1051–1060. https://doi.org/10.2174/1573399811666150615144707.
19. Perez-Inestrosa E, Suau R, Montanez MI, Rodriguez R, Mayorga C, Torres MJ, Blanca M. 2005. Cephalosporin chemical reactivity and its immunological implications. Curr Opin Allergy Clin Immunol 5:323–330. https://doi.org/10.1097/01.all.0000173788.73401.69.
20. Pan X, He Y, Chen T, Chan KF, Zhao Y. 2017. Modified penicillin molecule with carbapenem-like stereochemistry specifically inhibits class C β-lactamases. Antimicrob Agents Chemother 61:e01288-17. https://doi.org/10.1128/AAC.01288-17.
21. Powers RA, Caselli E, Focia PJ, Prati F, Shoichet BK. 2001. Structures of ceftazidime and its transition-state analogue in complex with AmpC β-lactamase: implications for resistance mutations and inhibitor design. Biochemistry 40:9207–9214. https://doi.org/10.1021/bi0109358.
22. Lahiri SD, Johnstone MR, Ross PL, McLaughlin RE, Olivier NB, Alm RA. 2014. Avibactam and class C β-lactamases: mechanism of inhibition, conservation of the binding pocket, and implications for resistance. Antimicrob Agents Chemother 58:5704–5713. https://doi.org/10.1128/AAC.03057-14.
23. Lahiri SD, Mangani S, Durand-Reville T, Benvenuti M, De Luca F, Sanyal G, Docquier JD. 2013. Structural insight into potent broad-spectrum inhibition with reversible recyclization mechanism: avibactam in complex with CTX-M-15 and *Pseudomonas aeruginosa* AmpC β-lactamases. Antimicrob Agents Chemother 57:2496–2505. https://doi.org/10.1128/AAC.02247-12.
24. Nukaga M, Papp-Wallace KM, Hoshino T, Lefurgy ST, Bethel CR, Barnes MD, Zeiser ET, Johnson JK, Bonomo RA. 2018. Probing the mechanism of inactivation of the FOX-4 cephamycinase by avibactam. Antimicrob Agents Chemother 62:e02371-17. https://doi.org/10.1128/AAC.02371-17.
25. Pozzi C, Di Pisa F, De Luca F, Benvenuti M, Docquier JD, Mangani S. 2018. Atomic-resolution structure of a class C β-lactamase and its complex with avibactam. ChemMedChem 13:1437–1446. https://doi.org/10.1002/cmdc.201800213.
26. Yamaguchi Y, Sato G, Yamagata Y, Doi Y, Wachino J-i, Arakawa Y, Matsuda K, Kurosaki H. 2009. Structure of AmpC β-lactamase ($AmpC^{D}$) from an *Escherichia coli* clinical isolate with a tripeptide deletion (Gly286-Ser287-Asp288) in the H10 helix. Acta Crystallogr Sect F Struct Biol Cryst Commun 65:540–543. https://doi.org/10.1107/S1744309109014249.
27. Na JH, Cha SS. 2016. Structural basis for the extended substrate spectrum of AmpC BER and structure-guided discovery of the inhibition activity of citrate against the class C β-lactamases AmpC BER and CMY-10. Acta Crystallogr D Struct Biol 72:976–985. https://doi.org/10.1107/S2059798316011311.
28. Jacobs MR, Abdelhamed AM, Good CE, Rhoads DD, Hujer KM, Hujer AM, Domitrovic TN, Rudin SD, Richter SS, van Duin D, Kreiswirth BN, Greco C, Fouts DE, Bonomo RA. 2018. ARGONAUT-I: activity of cefiderocol (S-649266), a siderophore cephalosporin, against Gram-negative bacteria, including carbapenem-resistant nonfermenters and *Enterobacteriaceae* with defined extended-spectrum β-lactamases and carbapenemases. Antimicrob Agents Chemother 63:e01801-18. https://doi.org/10.1128/AAC.01801-18.
29. Kazmierczak KM, Tsuji M, Wise MG, Hackel M, Yamano Y, Echols R, Sahm DF. 2019. *In vitro* activity of cefiderocol, a siderophore cephalosporin, against a recent collection of clinically relevant carbapenem-nonsusceptible Gram-negative bacilli, including serine carbapenemase- and metallo-β-lactamase-producing isolates (SIDERO-WT-2014 Study). Int J Antimicrob Agents 53:177. https://doi.org/10.1016/j.ijantimicag.2018.10.007.-]
30. Hackel MA, Tsuji M, Yamano Y, Echols R, Karlowsky JA, Sahm DF. 2019. Reproducibility of broth microdilution MICs for the novel siderophore cephalosporin, cefiderocol, determined using iron-depleted cation-adjusted Mueller-Hinton broth. Diagn Microbiol Infect Dis 94:321–325. https://doi.org/10.1016/j.diagmicrobio.2019.03.003.
31. Sawai T, Takahashi I, Yamagishi S. 1978. Iodometric assay method for β-lactamase with various β-lactam antibiotics as the substrates. Antimicrob Agents Chemother 13:910–913. https://doi.org/10.1128/aac.13.6.910.
32. Kabsch W. 2010. XDS. Acta Crystallogr D Biol Crystallogr 66:125–132. https://doi.org/10.1107/S0907444909047337.
33. Vagin A, Teplyakov A. 2010. Molecular replacement with MOLREP. Acta Crystallogr D Biol Crystallogr 66:22–25. https://doi.org/10.1107/S0907444909042589.
34. Winn MD, Ballard CC, Cowtan KD, Dodson EJ, Emsley P, Evans PR, Keegan RM, Krissinel EB, Leslie AG, McCoy A, McNicholas SJ, Murshudov GN, Pannu NS, Potterton EA, Powell HR, Read RJ, Vagin A, Wilson KS. 2011. Overview of the CCP4 suite and current developments. Acta Crystallogr D Biol Crystallogr 67:235–242. https://doi.org/10.1107/S0907444910045749.
35. Emsley P, Lohkamp B, Scott WG, Cowtan K. 2010. Features and development of Coot. Acta Crystallogr D Biol Crystallogr 66:486–501. https://doi.org/10.1107/S0907444910007493.
36. Adams PD, Afonine PV, Bunkoczi G, Chen VB, Davis IW, Echols N, Headd JJ, Hung LW, Kapral GJ, Grosse-Kunstleve RW, McCoy AJ, Moriarty NW, Oeffner R, Read RJ, Richardson DC, Richardson JS, Terwilliger TC, Zwart PH. 2010. PHENIX: a comprehensive Python-based system for macromolecular structure solution. Acta Crystallogr D Biol Crystallogr 66:213–221. https://doi.org/10.1107/S0907444909052925.
37. Chen VB, Arendall WB, III, Headd JJ, Keedy DA, Immormino RM, Kapral GJ, Murray LW, Richardson JS, Richardson DC. 2010. MolProbity: all-atom structure validation for macromolecular crystallography. Acta Crystallogr D Biol Crystallogr 66:12–21. https://doi.org/10.1107/S0907444909042073.